Annales Societatis Geologorum Poloniae (2024), vol. 94: 287–296 https://doi.org/10.14241/asgp.2024.13

CHARACTERIZATION OF DETRITAL SEDIMENTS WITHIN A STALAGMITE: THEIR ORIGINS AND INFLUENCE ON STALAGMITE MORPHOLOGY

Muhsin EREN* **& Muhammetmyrat PALVANOV**

Department of Geological Engineering, Mersin University, TR-33343, Çiftlikköy, Mersin, Turkey;
e-mails: m_eren@yahoo.com, fizikmuha93@gmail.com
** Corresponding author*

Eren, M. & Pavlanov, M., 2024. Characterization of detrital sediments within a stalagmite: their origins and influence on stalagmite morphology. *Annales Societatis Geologorum Poloniae*, 94: 287–296.

Abstract: This study examines the detrital sediments within a stalagmite from Küpeli Cave in southern Turkey, investigating their origin and role in shaping the morphology of the stalagmite. Its longitudinal section displays distinct macroscopic layering with alternating light and dark layers. The former layers mainly comprise mosaic and columnar sparite calcite, whereas the latter layers primarily consist of carbonate grains. The detrital sediments, consisting of carbonate grains, are divided into coarse- and fine-grained sediments. The coarse-grained detrital sediments with a size of 0.02 to 0.65 mm predominate and are characterized by poor sorting, including large, rounded, and red sand grains. The fine-grained detrital sediments consist of grains ≤ 10 μm and are characterized by good sorting. The detrital sediments most likely were derived from red soils in surface karst depressions and primarily contained grains with angular and etched boundaries caused by the chemical weathering of bedrock carbonates. The rounded large sand grains are thought to have entered the soil zone by wind or surface runoff before being incorporated into the stalagmite. Dripping water carried these carbonate grains into the cave, depositing them in depressions caused by solution processes at the top of the stalagmite during its formation. Under sediment displacement towards the periphery occurred within these depressions, owing to water splash action, forming slight elevations. This mechanism contributed significantly to the stalagmite's distinctive appearance, resembling a partially burnt candle. The alternating calcite and detrital sediment layers reflect recurring climatic conditions, with the detrital sediments deposited during increased rainfall and the calcite layers formed during drier periods with minimal clastic input and increased evaporation. The fine-grained detrital sediments further indicate formation during drier periods with significantly reduced rainfall.

Key words: Speleothem, stalagmite, calcite, detrital sediment, Küpeli cave, Turkey.

Manuscript received 15 November 2023, accepted 9 September 2024

INTRODUCTION

Speleothems, comprising stalactites, stalagmites, and flowstones, are intriguing formations, found in caves primarily made up of calcite and aragonite precipitated from calcium carbonate-rich percolating water. The significance of speleothems, particularly stalagmites, in paleoclimatic reconstructions has attracted considerable attention worldwide (Bar-Matthews *et al*., 1997, 2010; McDermott, 2004; Dominguez-Villar *et al*., 2008; Tremaine *et al*., 2011; Voarintsoa *et al*., 2017), with Turkey notably contributing to this field (Fleitmann *et al*., 2009; Göktürk *et al*., 2011; Rowe *et al*., 2012; Ünal-İmer, 2015; Ünal-İmer *et al*., 2015, 2016). Furthermore, previous studies in Turkey have addressed various facets of cave and speleothem research, such as karst evolution in the region, with numerous cave descriptions by Akgöz (2012), growth axis angle deviations in stalagmites dated by the U/Th method and their relationship with palaeoseismology by Akgöz and Eren (2015), properties of calcite precipitated from a thin layer of water taken from the surface of stalagmites by Eren *et al*. (2017), primary features of selected stalagmites by Eren *et al*. (2021), micro-karstification features in a stalagmite by Eren *et al*. (2022), and chemical composition of calcite crystals and pore-filling sediments in a stalagmite determined using electron-probe microanalysis (EPMA) by Palvanov *et al*. (2024). Eren *et al*. (2017, 2022) and Palvanov *et al*. (2024) have conducted studies linked to Küpeli Cave. However, research on the detrital sediments interbedded with chemically precipitated calcite layers within speleothems remains relatively limited (Railsback *et al*.,

1999; Auler *et al*., 2009; Dasgupta *et al*., 2010; Pickering *et al*., 2010; Denniston and Luetscher 2017). Detrital sediments in speleothems originate from diverse sources, often carried into caves by wind (White, 1988; Railsback *et al*., 1999), flooding (Dasgupta *et al*., 2010; Lascu and Feinberg, 2011; Finné *et al*., 2014; Gázquez *et al*., 2014; González-Lemos *et al*., 2015; Denniston and Luetscher, 2017; Sala and Bella, 2023), and dripping waters (Railsback *et al*., 1999; Lascu and Feinberg, 2011; Schimpf *et al*., 2011; Zupančič *et al*., 2016; Belli *et al*., 2017). This study aims to characterize the detrital sediments deposited as a layer on a stalagmite, to investigate their origins, and, for the first time, to examine their influence on stalagmite morphology.

GEOLOGICAL AND SPELEOLOGICAL SETTING

Küpeli Cave is located in the northeast of Esenpınar (Erdemli/Mersin), a small settlement in southern Turkey (Fig. 1A). The cave entrance is at 59.9726°E latitude and 40.51941°N longitude (UTM: 34.114917°E and 36.606085°N), at an altitude of 742 m above sea level. The cave is nestled within the central part of the Tauride orogenic belt, which is largely defined by platform carbonates (Fig. 1B; Özgül, 1984). Most caves in this area, including Küpeli Cave, are found within the reefal limestones of the Mut Formation (Langian–Serravian), also referred to as the Karaisalı Formation, known for its abundance of red algae and corals (Gedik *et al*., 1979; Eren, 2008; Akgöz, 2012; Akgöz and Eren, 2015). The regional climate is typically Mediterranean, characterized by an average annual precipitation of 550 mm, evaporation of 1296 mm, and an average temperature of 18.7°C, based on the 39-year meteorological records from the Turkish State Meteorological Service (2020).

Küpeli Cave comprises two chambers, connected by a narrow passage (Fig. 2A), with an estimated overburden thickness of 30–50 cm for the soil cover and 6 to 10 m for the epikarst zone. The first chamber is 30 x 20 m in size and has a height of 0.4 to 28 m. Access to this chamber is via a ladder from the collapsed part of the roof, which measures 4.9 x10 m. The second chamber, smaller than the first, is 17 m long, 9 m wide and 38 m high. The first chamber features small stalagmites with milky white tops and moist surfaces, possibly indicating ongoing stalagmite formation processes.

MATERIALS AND METHODS

The stalagmite sample was selected for its distinct detrital layers evident on the longitudinal cut surface. A parallel slice was then cut from half of the stalagmite, ensuring comprehensive coverage. Eight thin sections were prepared to capture details and were examined under a polarized microscope.

Scanning electron microscopy coupled with energy-dispersive X-ray spectroscopy (SEM-EDS) was performed at Çukurova University (Adana, Turkey), using a JEOL JSM 84A device on the two samples taken from calcite and detrital sediment layers. The samples were obtained from the layers by first cutting off a piece and then breaking it to the required size. The mineralogical composition of two bulk samples, extracted from the detrital and calcite layers using cutting and a dental drill, was analyzed by X-ray diffraction (XRD) at the Mersin University Advanced Technology Education, Research, and Application Center (MEITAM) in Turkey. The XRD measurements were conducted on a Rigaku D/Max–2200 Ultia PC instrument, employing CuKα radiation. The scanning speed for data collection was set at $1^{o}2\theta$ min^{-1}.

RESULTS

Stalagmite description

The stalagmite in the growth position was 101 cm long and 6–35 cm wide, with a truncated cone shape and a depression at the top (Fig. 2B). For this study, a sample was taken from the uppermost part of the stalagmite, which is approximately 25 cm long (Fig. 2C). The stalagmite's outer surface is brown, with a knotty structure (Fig. 2C). The depression at the top is 4.5 cm wide and 1 to 2 mm deep (Fig. 2C). The longitudinal cut shows a macroscopic layering of light and dark layers, with a thickness typically of 1 to 5 mm, up to 1 cm (Fig. 2D). The alternating undulating layers give the stalagmite the appearance of a partially burnt candle, which also was preserved during its progressive growth (Fig. 2D). The layers flatten or bend slightly downward in the middle. The thickness of the detrital layers increases on both sides of the central part, forming slight elevations and being more inclined at the flanks (Fig. 2D). In contrast to the detrital layers, the calcite layers are thick in the centre of the stalagmite, somewhat thinner in the areas of detrital sediment elevation, and end with a thinning at the flanks. The trace of the macro-hole, which begins in the depression at the top of the stalagmite and extends diagonally below it, is visible in the section parallel to the longitudinal half-section (Fig. 2E). The macro-hole on the cut surface has the cross-section of a lens, measuring about 2 cm long and less than 0.5 cm wide, and it is partially filled with internal sediment (Fig. 2E). Figure 2F shows a close-up of detrital sediment, consisting of grains with angular and etched boundaries.

Petrography

Petrographic analysis of thin sections shows that the alternating microlayers consist primarily of a mosaic of sparite calcite crystals and detrital carbonate sediments (Fig. 3). Furthermore, columnar calcite is occasionally present within the calcite microlayers, consisting of elongate, roughly parallel crystals (Fig. 3 B). The term "columnar" is used for elongated calcite crystals, the dimensions of which are defined as columnar according to Kendall and Broughton (1978), and short columnar according to Frisia and Borsato (2010). The calcite microlayers represent light-coloured growth microlayers in the stalagmite whereas the detrital sediments form dark microlayers (Fig. 3). In the calcite microlayers, the mosaic calcite crystals have a diameter of 0.05–0.10 mm, while the columnar calcite crystals are about

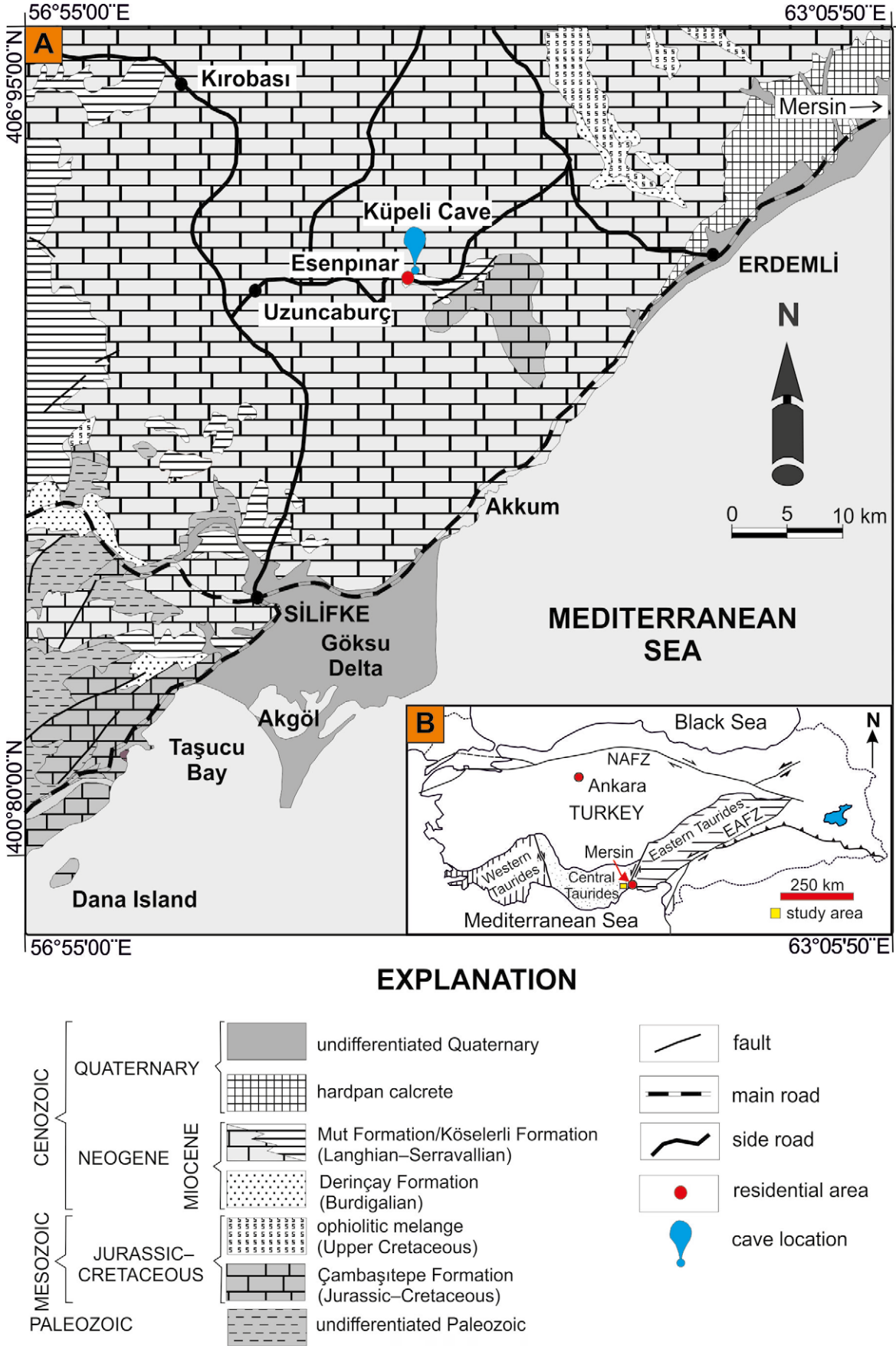

Fig. 1. Study site. **A.** Geological map of the study area showing the cave location (adapted from Gedik *et al*., 1979; Eren *et al*., 2022). **B.** Subdivisions of the Tauride Orogenic Belt, indicating the study area position within the central part (adapted from Özgül, 1984; Eren *et al*., 2022).

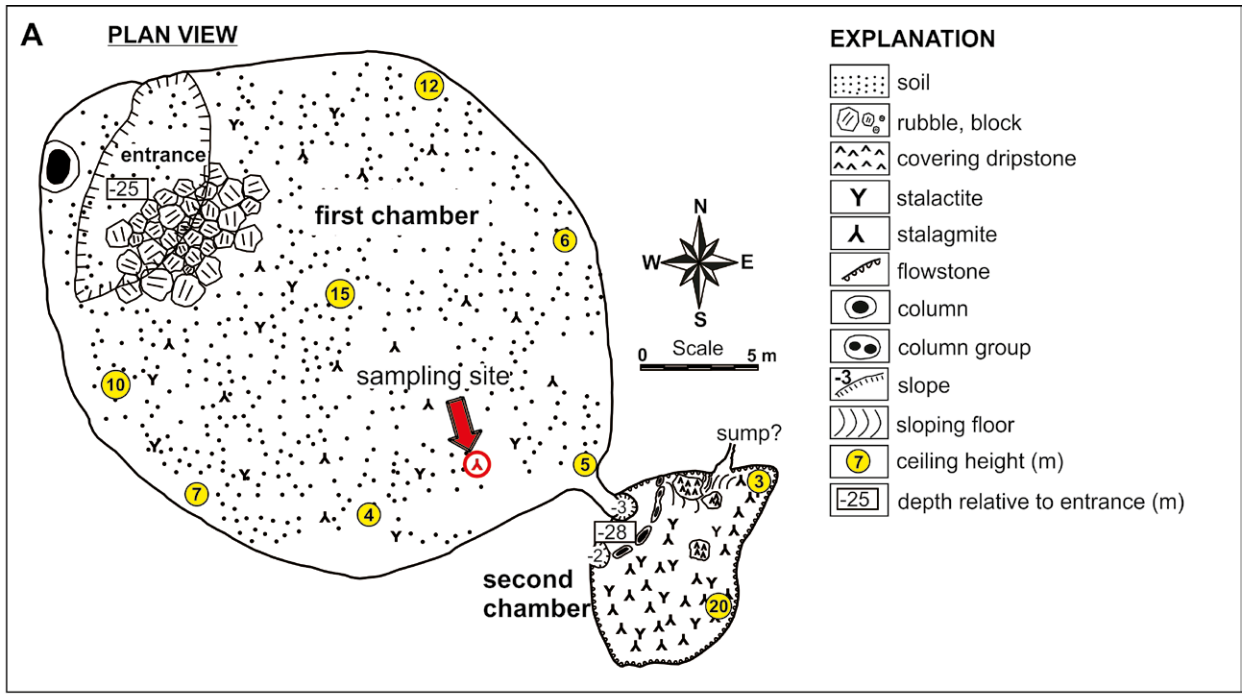

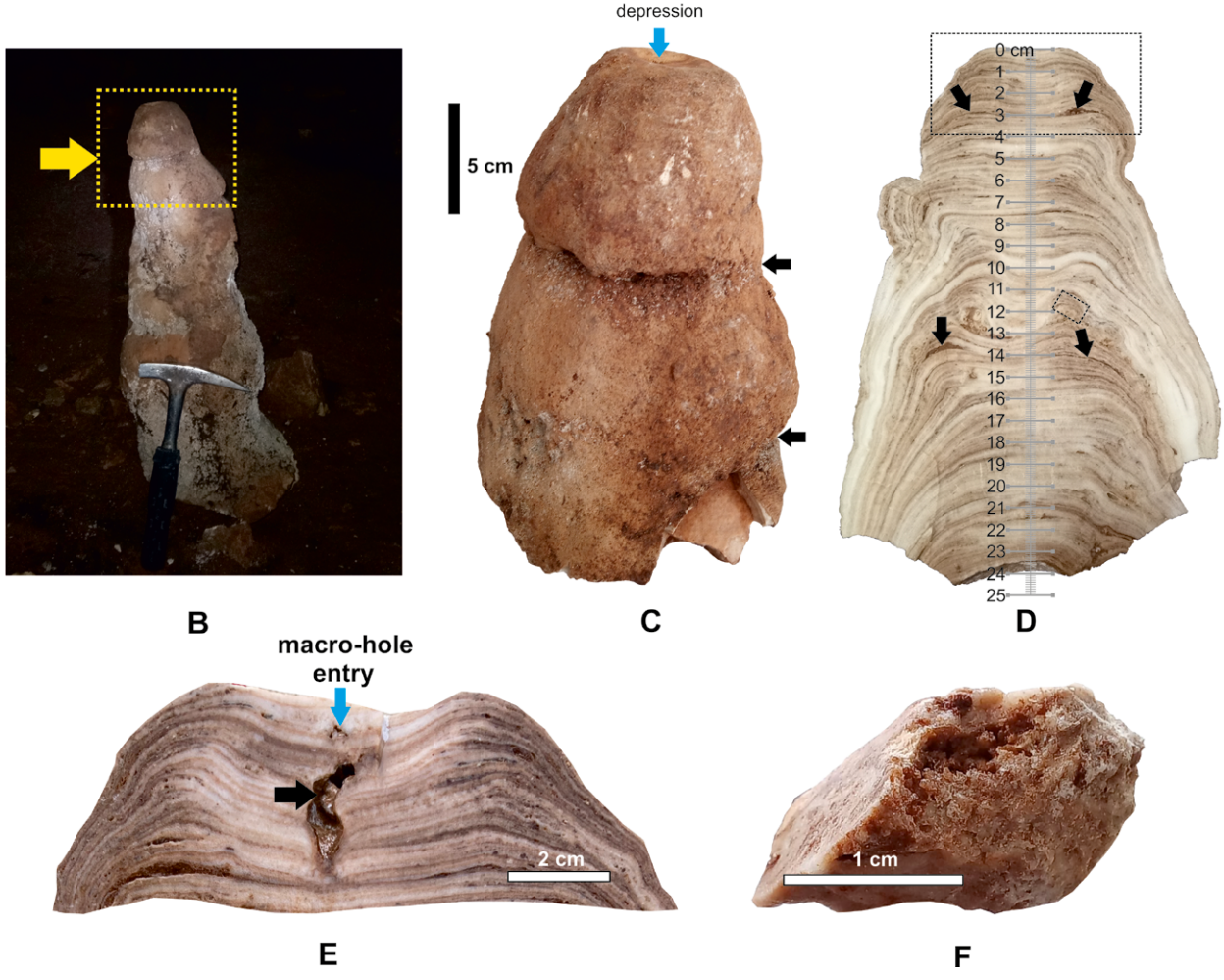

Fig. 2. Cave and stalagmite details. **A.** Plan view of the Küpeli Cave (adapted from Akgöz, 2012; Eren *et al*., 2022). **B.** The stalagmite is in a growth position within the cave**. C.** Close-up of the marked section in (B) showing dissolution depression (blue arrow) and knotted structure (black arrows). **D.** Longitudinal half section with light-dark microlayers and detrital sediment elevations (black arrows). **E.** Macro-hole on the sliced surface of the uppermost part of the stalagmite parallel to the longitudinal half section (large frame in D), reaching the current apex depression (blue arrow), crossing the layering, and containing internal sediments (black arrow). **F.** Close-up of a slight elevation where detrital sediments are concentrated in the small frame in (D).

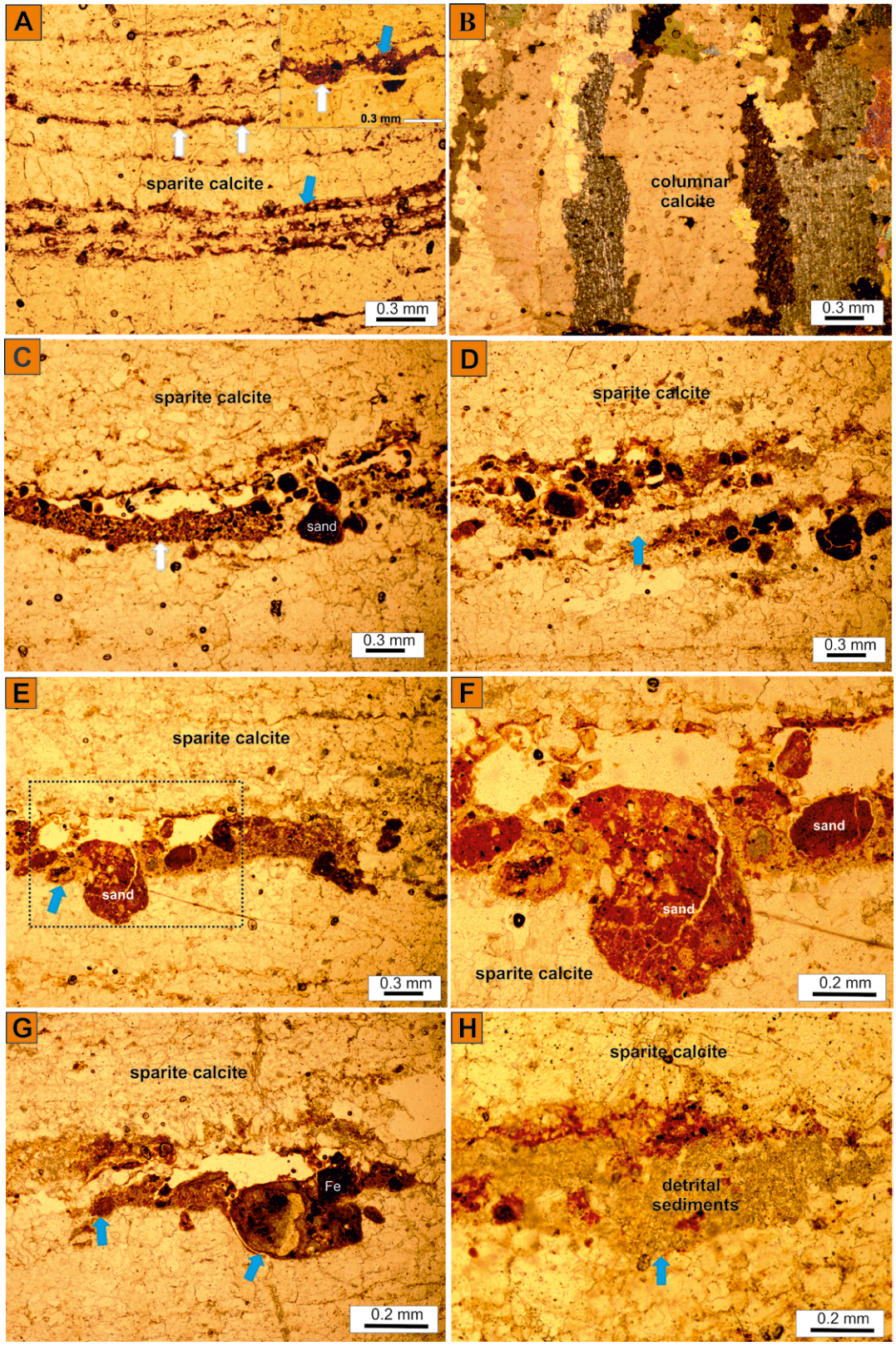

Fig. 3. Photomicrographs. **A.** Alternating layers of mosaic sparite calcite and fine-grained detrital sediments. Micro-scale corrosion pits are indicated by white arrows, while blue arrows highlight angular to rounded grains of fine-grained detrital sediment. **B.** Columnar calcite microfabric with elongated calcite crystals. **C.** Coarse-grained detrital sediment composed of carbonate grains filling corrosion depression (white arrow) exhibiting poor sorting and abundant red colouration. Red colouration and roundness are more evident in the sand grains. **D.** Recrystallization in the detrital sediment transforming silt-sized carbonate grains into sparite calcite (blue arrow). **E.** Common large micritic limestone grains with red colour and rounded morphology in coarse-grained detrital sediments. The blue arrow indicates the corrosion surface. **F.** Close-up of the frame in (E). **G.** Coarse-grained detrital sediments overlying the corrosion surface (blue arrows) of the calcite layer with visible Fe-oxide minerals. **H.** Fine-grained detrital sediments composed of angular to subangular carbonate grains. The blue arrow indicates the corrosion surface. The micrograph (B) is under polarized light, and the others are under normal light.

0.2–0.6 mm wide and up to 1.2 mm long. Their surfaces covered with detrital sediments often show micro-scale corrosion pits (Fig. 3A, C–H).

Under microscopic examination, the detrital sediments can be classified into two distinct categories: (i) poorly sorted coarse-grained detrital sediments, with grain sizes ranging from 0.02 to 0.65 mm (Fig. 3C–G); and (ii) fine-grained detrital sediments, consisting of particles with diameters ≤ 10 µm (Fig. 3A, H). Notably, the large sand grains exhibit a prominent dark red colouration and roundness (Fig. 3C–G). Furthermore, certain detrital sediments have undergone partial recrystallization into sparite calcite, causing disruptions in the initial granular texture, with coarse sand grains appearing to resist recrystallization (Fig. 3D).

SEM-EDS analysis

SEM analysis shows that the calcite growth layers consist primarily of euhedral and subhedral calcite crystals (Fig. 4A). Moreover, within these layers, there are intercrystalline pores that have been enlarged, owing to dissolution processes (Fig. 4A). The remains of fine-grained detrital sediments on the partially dissolved surface of the larger calcite crystals appear as carbonate grains with angular and etched boundaries (Fig. 5B). Examination of the EDS spectra confirms the presence of calcite crystals in the growth and fine-grained detrital sediment layers, with a strong Ca peak (Fig. 5C, D).

XRD analysis

X-ray diffraction analysis shows that the light-coloured growth layers consist entirely of calcite (Fig. 5A). In contrast, the darker layers, which are rich in detrital sediments, consist predominantly of calcite with a negligible presence of quartz (<1 wt%; Fig. 6B). The identification of quartz was confirmed by its distinctive peak at 3.36 Å (Fig. 5B).

DISCUSSION

The stalagmite from Küpeli Cave has remarkable detrital microlayers recurring with sparite calcite microlayers, including columnar calcite (Fig. 2D). The petrographic analyses reveal that the detrital microlayers predominantly consist of carbonate grains of similar composition (Fig. 3). This indicates that these grains were transported from the same source by dripping water. Notably, the absence of layered detrital sediments in other stalagmites within the same cave indicates that the conditions are specific

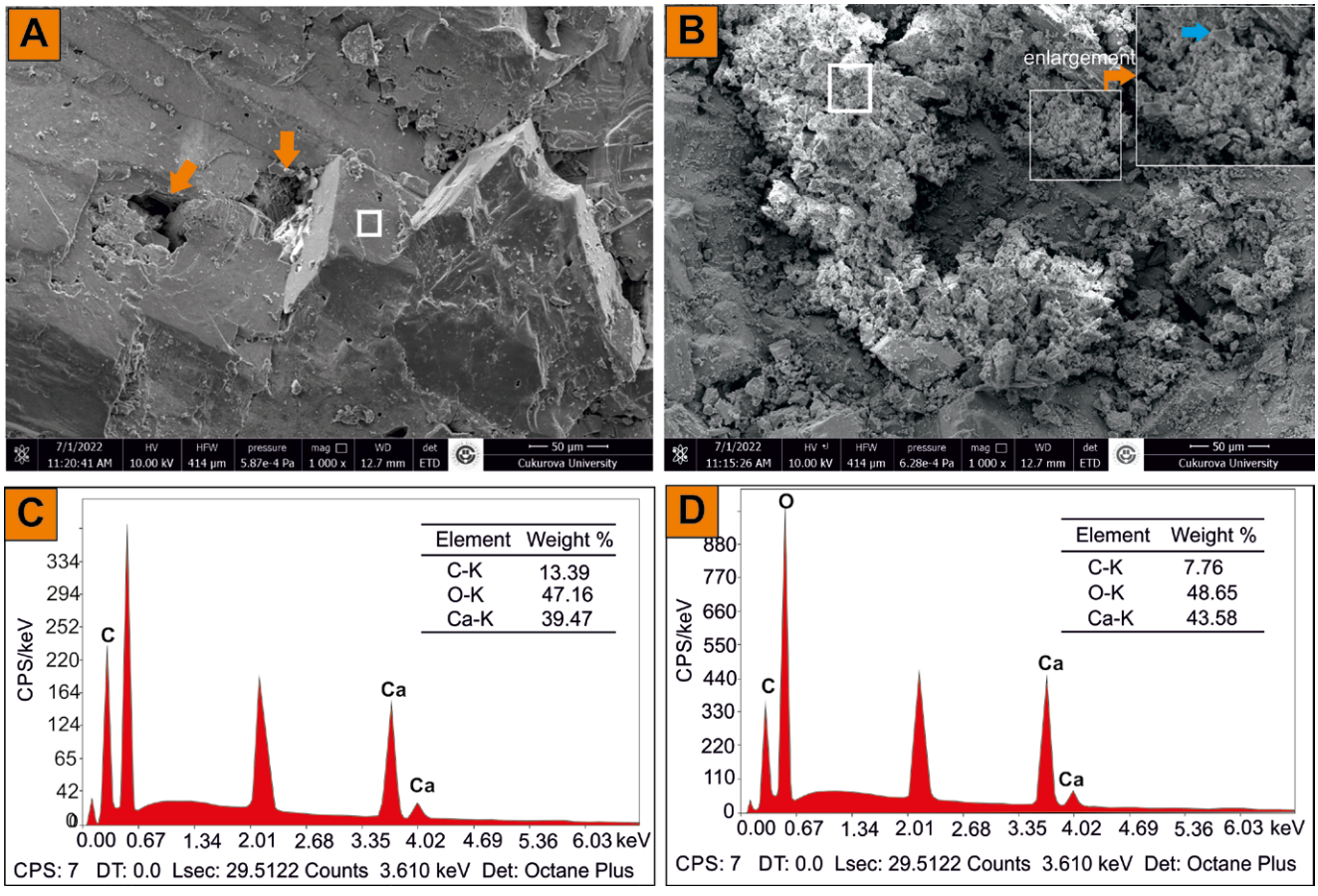

Fig. 4. SEM images with EDS spectra. **A.** Sparite calcite crystals within the growth layer, exhibit intercrystalline pores partially enlarged by dissolution (orange arrows). **B.** Remnants of a fine-grained detrital sediment layer containing carbonate grains, characterized by angular and etched boundaries (indicated by a blue arrow within the enlarged frame marked by an orange arrow). **C.** EDS spectrum of large calcite crystal in A. **D.** EDS spectrum of fine-grained detrital sediments in B. Thick white frames in A and B indicate areas analyzed by EDS.

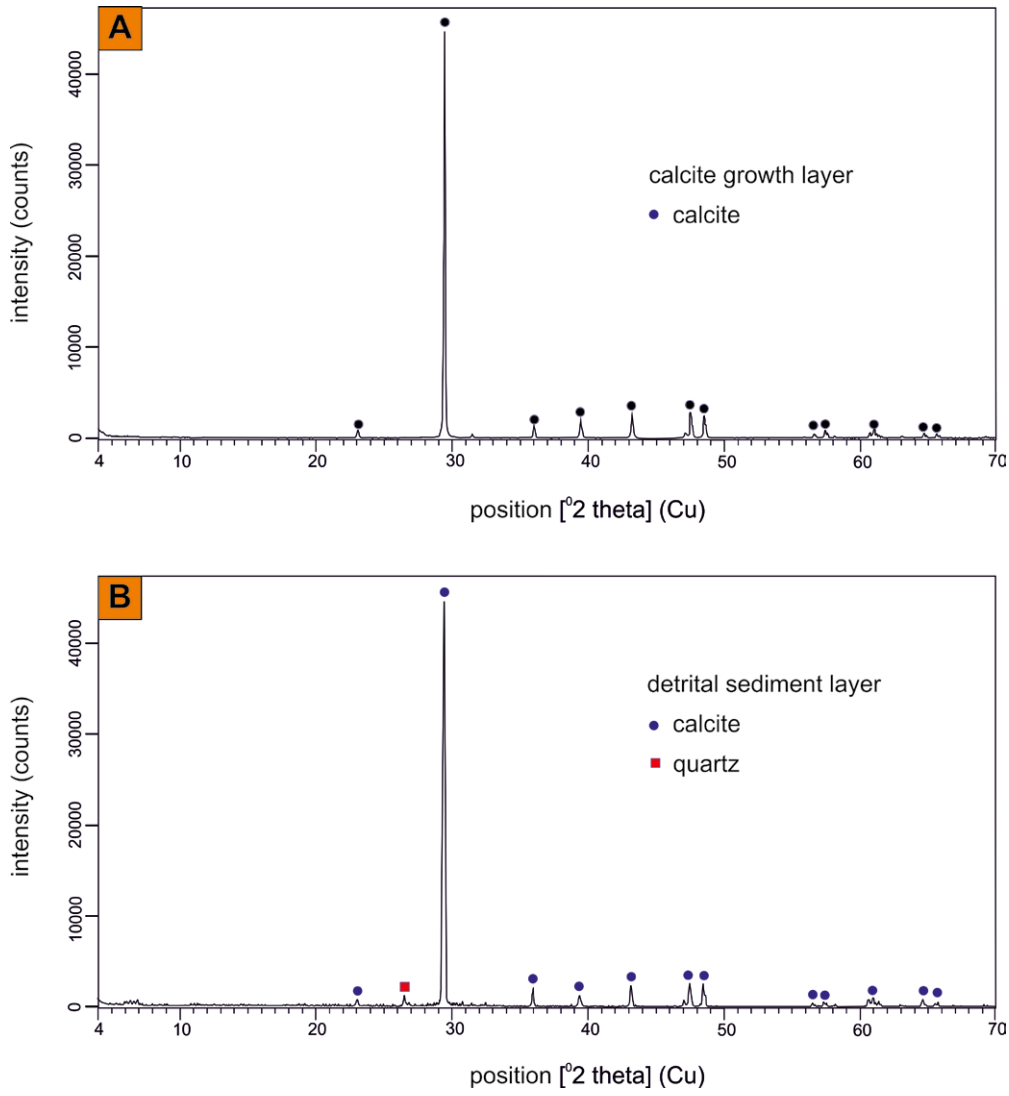

Fig. 5. X-ray diffractograms. **A.** Calcite growth layers consist entirely of calcite. **B.** Detrital sediment layers are primarily calcite with a small amount of quartz (<1 wt%).

to this stalagmite (e.g., Eren *et al*., 2022; Palvanov *et al*., 2024). The presence of rounded grains within the detrital sediments (Fig. 3C–G), coupled with the prevalence of red coloration, indicates their likely origin from the red soils, found in the surface karst depressions (doline and uvala), formed by chemical weathering of the bedrock. These red soils are primarily composed of insoluble residues remaining after the dissolution of the bedrock carbonates. This interpretation receives further support from the abundance of angular and etched boundaries observed in the transported grains (Figs 2F, 4B). While the red colouration is commonly associated with the presence of Fe-oxide minerals (Eren and Kadir, 1999; Eren *et al*., 2015), notably absent in the XRD diffractogram (Fig. 5B), it indicates a connection with mineral crystallinity and the potential presence of non-crystalline Fe-hydroxide minerals (White, 2007). The rounded sand-sized carbonate grains in the soils indicate a previous local transport of the grains by wind (Railsback *et al*., 1999) or by surface runoff. In addition, the presence of a very small quartz peak in the XRD diffractogram of the detrital sediments (Fig. 5B),

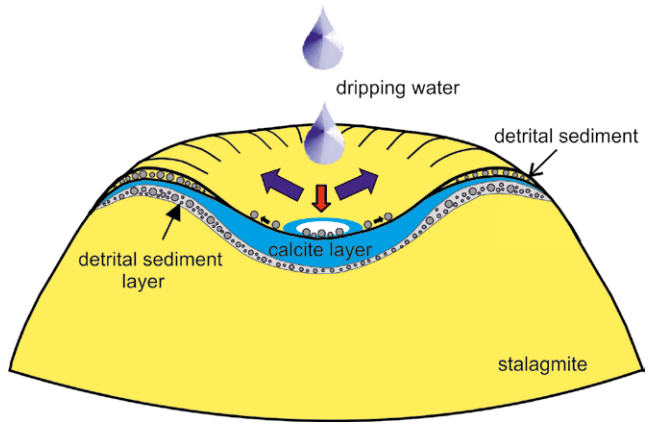

Fig. 6. Schematic representation of the process of detrital sediment deposition in a depression generated by dissolution over time at the top of the stalagmite and its effect on stalagmite morphology. The splashing action of the dripping water drives the grains towards the edges of the stalagmite, causing an increase in sediment accumulation in these areas. Subsequently, under favorable conditions, calcite precipitates in the depression and takes its shape by filling the remaining space.

coupled with the lack of supporting evidence in the other analyses, may indicate that a negligible quantity of silt and finer quartz particles could have been deposited in the soil environment by wind transport. These red soils probably were formed at the same time as the cave. The results indicate that the process of introduction of detrital sediments into the cave began in the red soil zone at the surface, continued through the cracks in the epikarst area, and finally penetrated the cave system. This explains one mechanism by which sediment was transported from the surface into the cave environment; the other was as gravitational debris, which is the coarser-grained material (White, 2007).

In the longitudinal section, the tapering of the detrital layers towards the centre of the stalagmite and a slight elevation at the sides (Fig. 2D) indicate deposition in depressions caused by dissolution processes at the top of the stalagmite during its formation (Fig. 2C, E). A similar depression exists at the top of the stalagmite connected with the macro-hole below it (Fig. 2E). The macro-hole is partially filled with internal sediments transported from the depression inside to the stalagmite by the percolation of water (Fig. 2E). The formation of macro-holes in stalagmites has been studied in detail by Shtober-Zisu *et al*. (2014); they concluded that the dissolution process could be enhanced or even triggered by bacteria, present in stalagmites. However, no evidence of microbial origin was found in this study. Consequently, it indicates that inorganic processes are the probable mechanisms for dissolution.

The detrital sediment distribution in the apex depressions was caused by the splashing action of dripping water pushing grains to the sides, resulting in increased accumulation in those areas (Fig. 6). This mechanism, together with dissolution, contributed to the stalagmite's distinctive appearance, similar to the rimmed top of a partially burnt candle (Fig. 2D) throughout its development (Martín-Chivelet *et al*., 2017). Furthermore, the detrital sediments, composed of micritic limestone particles, have undergone partial recrystallization and transformation into sparite calcite during the onset of calcite precipitation (Fig. 3D). Notably, larger grains seem to have been protected from this transformative process (Fig 4D). This recrystallization process has altered the original granular texture of clastic sediments into a crystalline one (Fig. 3D).

After the deposition of the detrital sediments, calcite was precipitated from the water film to form a new calcite growth microlayer covering the speleothem (Fig. 6). It took the shape of the depression remaining after detrital sediment accumulation. Therefore, the calcite layers are thick at the centre of the stalagmite, gradually tapering over the detrital sediment elevation zones, and finally thinning out towards the flanks. The calcite layer surfaces beneath the detrital sediments, often showing corrosion pits (Fig 3), corresponding to a change in water composition and the presence of a hiatus, also have been reported in the literature (Finné *et al*., 2014; Sala and Bella, 2023). The amount and composition of drip water are subject to significant variations driven by seasonal changes in climatic conditions. Rainy seasons are characterized by increased detrital input, influenced by the carrying capacity of rainwater, while drier periods witness reduced detrital input or even cessation of grain supplies. In rainy seasons, the shorter retention times of rainwater in the soil and epikarst areas enhance the absorption of CO_2 in the soil, yet indicate insufficient interaction time for the dissolution of carbonate components. This implies that the water carrying the detrital grains was undersaturated with calcite, which increased its aggressiveness toward carbonates and facilitated the formation of solution pits on the surface of the calcite layers. (Railsback *et al*., 2011, 2013; Sala and Bella, 2023). Conversely, drier seasons coincide with chemical precipitation events, with minimal detrital input (Lascu and Feinberg, 2011). Railsback *et al*. (2011) also suggest moderate climatic conditions for calcite precipitation. Factors such as temperature, humidity, and pCO_2 levels influence calcite precipitation (Day and Henderson, 2011), with weak rainfall prolonging the interaction time in soil and epikarst regions, leading to increased water saturation for calcite and subsequent calcite precipitation. Increased evaporation and degassing during dry periods contributed to higher water saturation levels, triggering chemical precipitation of calcite layers and reducing grain transport or halting flow altogether.

CONCLUSION

Detrital sediments in the stalagmite are interlayered with chemically precipitated calcite microlayers. These sediments are mainly composed of red, sandy-silty carbonate grains along with finer detrital carbonate particles. The well-rounded sand grains in the sediments indicate earlier transportation, possibly by wind or runoff. These sediments were formed from red soils caused by chemical and physical weathering processes on the carbonate rocks at the surface. Over time, these weathered particles were carried into the cave environment by dripping water and deposited in depressions, formed by dissolution at the top during stalagmite development. Subsequently, the sediments were moved toward the edge of the depression by the splashing action of dripping water, resulting in a slight elevation and an increase in sediment concentration. As a result of this process, the stalagmite expanded laterally and acquired the appearance of the edge of a partially burnt candle. Afterward, the chemically precipitated calcite microlayer took on the shape of the depression at the top of the stalagmite. The detrital and chemically precipitated microlayers may have recurred in response to seasonal climate changes. The amount and size of sediment grains increased, depending on the amount of rainfall, and during dry periods, chemical precipitation occurred from supersaturated water in the absence of sediment input.

Acknowledgments

The authors express their sincere gratitude to Loren Bruce Railsback from the Geology Department at the University of Georgia and the anonymous reviewer for their insightful and constructive feedback. Their insights significantly enhanced the quality of this paper.

REFERENCES

Akgöz, M., 2012. *Göksu nehri ve Lamas kanyonu (Mersin) arasında kalan bölgenin karst evrimi*. Unpublished Ph.D. Thesis, Mersin University, Turkey, 290 pp. [In Turkish.]

Akgöz, M. & Eren, M., 2015. Traces of earthquakes in the caves: Sakarlak Ponor and Kepez Cave, Mersin (S Turkey). *Journal of Cave and Karst Studies*, 77: 63–74.

Auler, A. S., Smart, P. L., Wang, X., Piló, L. B., Edwards, R. L. & Cheng, H., 2009. Cyclic sedimentation in Brazilian caves: Mechanisms and palaeoenvironmental significance. *Geomorphology*, 106: 142–153.

Bar-Matthews, M., Ayalon, A. & Kaufman, A., 1997. Late Quaternary palaeoclimate in the eastern Mediterranean region from stable isotope analysis of speleothems at Soreq Cave, Israel. *Quaternary Research*, 47: 155–168.

Bar-Matthews, M., Marean, C. W., Jacobs, Z., Karkanas, P., Fisher, E. C., Herries, A. I., Brown, K., Williams, H. M., Bernatchez, J., Ayalon, A. & Nilssen, P. J., 2010. A high-resolution and continuous isotopic speleothem record of paleoclimate and paleoenvironment from 90 to 53 ka from Pinnacle Point on the south coast of South Africa. *Quaternary Science Reviews*, 29: 2131–2145.

Belli, R., Borsato, A., Frisia, S., Drysdale, R., Maas, R. & Greig, A., 2017. Investigating the hydrological significance of stalagmite chemical (Mg, Sr) using Sr isotope and particulate element records across the Late Glacial-to-Holocene transition. *Geochimica Cosmochimica Acta*, 199: 247–263.

Dasgupta, S., Saar, M. O., Edwards, L., Shen, C. C., Cheng, H. & Alexander, E. C., 2010. Three thousand years of extreme rainfall events recorded in stalagmites from Spring Valley Caverns, Minnesota. *Earth and Planetary Science Letters*, 300: 46–54.

Day, C. C. & Henderson, G. M., 2011. Oxygen isotopes in calcite grown under cave-analogue conditions. *Geochimica et Cosmochimica Acta*, 75: 3956–3972.

Denniston, R. F. & Luetscher, M., 2017. Speleothems as high-resolution paleo flood archives. *Quaternary Science Reviews*, 170: 1–13.

Domínguez-Villar, D., Wang, X., Cheng, H., Martín-Chivelet, J. & Edwards, R. L., 2008. A high-resolution late Holocene speleothem record from Kaite Cave, northern Spain: $\delta^{18}O$ variability and possible causes. *Quaternary International*, 187: 40–51.

Eren, M., 2008. Olba (Ura-Uğuralanı) jeoarkeolojisi (Silifke, Mersin). *Ankara, Kültür ve Turizm Bakanlığı 24. Arkeometri Sonuçları Toplantısı*, pp. 181–192. [In Turkish.]

Eren, M., Akgöz, M., Kadir, S. & Kapur, S., 2021. Primary characteristics of selected stalagmites from four caves located between Erdemli and Silifke (Mersin), southern Turkey–implications on their formation. *Carbonates and Evaporites*, 36: 2.

Eren, M. & Kadir, S., 1999. Colour origin of upper Cretaceous pelagic red sediments within the eastern Pontides, northeast Turkey. *International Journal of Earth Sciences*, 88: 593–595.

Eren, M., Kadir, S. & Akgöz, M., 2017. Mineralogical, geochemical and micromorphological characteristics of calcite precipitated from a thin cover of recent water taken from the stalagmites in Küpeli Cave, Esenpınar (Erdemli, Mersin), southern Turkey. *Turkish Journal of Engineering*, 1: 1–8.

Eren, M., Kadir, S., Kapur, S., Huggett, J. & Zucca, K., 2015. Colour origin of Tortonian red mudstones within the Mersin area, southern Turkey. *Sedimentary Geology*, 318: 10–19.

Eren, M., Palvanov, M., Kadir, S. & Kapur, S., 2022. Microkarstification in a stalagmite, Küpeli Cave, southern Turkey. *Acta Carsologica*, 51: 5–19.

Finné, M., Bar-Matthews, M., Holmgren, K., Sundqvist, H. S., Liakopoulos, I. & Zhang, Q., 2014. Speleothem evidence for late Holocene climate variability and floods in Southern Greece. *Quaternary Research*, 81: 213–227.

Fleitmann, D., Cheng, H., Badertscher, S., Edwards, R. L., Mudelsee, M., Göktürk, O. M., Fankhauser, A., Pickering, R., Raible, C. C., Matter, A., Kramers, J. & Tüysüz, O., 2009. Timing and climatic impact of Greenland interstadials recorded in stalagmites from northern Turkey. *Geophysical Research Letters*, 36: L19707.

Frisia, S. & Borsato, A., 2010. Karst. In: Alonso-Zarza, A. M. & Tanner, L. H. (eds), *Carbonates in Continental Settings: Facies, Environments, and Processes. Developments in Sedimentology*, 61: 269–318.

Gázquez, F., Calaforra, J. M., Forti, P., Stoll, H., Ghaleb, B. & Delgado-Huertas, A., 2014. Paleoflood events recorded by speleothems in caves. *Earth Surface Processes and Landforms*, 39: 1345–1353.

Gedik, A., Birgili, Ş., Yılmaz, H. & Yoldaş, R., 1979. Geology of the Mut- Ermenek- SiMfke (Konya, Mersin) area and petroleum possibilities. *Bulletin of the Geological Society of Turkey*, 22: 7–26. [In Turkish.]

González-Lemos, S., Jiménez-Sánchez, M. & Stoll, H. M., 2015. Sediment transport during recent cave flooding events and characterization of speleothem archives of past flooding. *Geomorphology*, 228: 87–100.

Göktürk, O. M., Fleitmann, D., Badertscher, S., Cheng, H., Edwards, R. L., Fankhauser, A., Tüysüz, O. & Kramers, J., 2011. Climate on the southern Black Sea coast during the Holocene: implications from the Sofular Cave record. *Quaternary Science Reviews*, 30: 2433–2445.

Kendall, A. C. & Broughton, P. L., 1978. Origin of fabrics in speleothems composed of columnar calcite crystals. *Journal of Sedimentary Petrology*, 48: 519–538.

Lascu, I. & Feinberg, J. M., 2011. Speleothem magnetism. *Quaternary Science Reviews*, 30: 3306–3320.

Martín-Chivelet, J., Muñoz-García, M. B., Cruz, J. A., Ortega, A. I. & Turrero, M., 2017. Speleothem architectural analysis: Integrated approach for stalagmite-based paleoclimate research. *Sedimentary Geology*, 353: 28–45.

McDermott, F., 2004. Palaeo-climate reconstruction from stable isotope variations in speleothems: a review. *Quaternary Science Reviews*, 23: 901–918.

Özgül, N., 1984. Stratigraphic and tectonic evolution of the central Taurides. In: Tekeli, O. & Göncüoğlu, M. C. (eds), *Geology of the Taurus Belt. Proceedings of International Tauride Symposium. Mineral Research and Exploration Institute (MTA), Turkey, Special Publication*, pp. 77–90.

Palvanov, M., Eren, M. & Kadir, S., 2024. EPMA Analysis of a stalagmite from Küpeli Cave, southern Turkey: implications on detrital sediments. *Carbonates and Evaporites*, 39: 3.

Pickering, R., Kramers, J. D., Partridge, T., Kodolanyi, J. & Pettke, T., 2010. U-Pb dating of calcite–aragonite layers in

speleothems from hominin sites in South Africa by MC-ICP-MS. *Quaternary Geochronology*, 5: 544–558.

Railsback, L. B., Akers, P. D., Wang, L., Holdridge, G. A. & Voarintsoa, N. R., 2013. Layer bounding surfaces in stalagmites as keys to better paleoclimatological histories and chronologies. *International Journal of Speleology*, 42: 167–180.

Railsback, B. L., Brook, G. A. & Webster, J. W., 1999. Petrology and paleoenvironmental significance of detrital sand and silt in a stalagmite from Drotsky's cave, Botswana. *Physical Geography*, 20: 331–347.

Railsback, L. B., Liang, F., Vidal Romaní, J. R., Grandal-d'Anglade, A., Vaqueiro Rodríguez, M., Santos Fidalgo, L., Fernández Mosquera, D., Cheng, H. & Edwards, R. L., 2011. Petrographic and isotopic evidence for Holocene long-term climate change and shorter-term environmental shifts from a stalagmite from the Serra do Courel of northwestern Spain and implications for climatic history across Europe and the Mediterranean. *Palaeogeography, Palaeoclimatology, Palaeoecology*, 305: 172–184.

Rowe, P. J., Mason, J. E., Andrews, J. E., Marca, A. D., Thomas, L., Calsteren, P. V., Jex, C. N., Vonhof, H. B. & Al-Omari, S., 2012. Speleothem isotopic evidence of winter rainfall variability in northeast Turkey between 77 and 6 ka. *Quaternary Science Reviews*, 45: 60–72.

Sala, P. & Bella, P., 2023. Corrosion of carbonate speleothems by an allogenic river inferred from petrography and a weight loss experiment: a case study from the Demänová Cave System, Slovakia. *Annales Societatis Geologorum Poloniae*, 93: 467–481.

Schimpf, D., Kilian, R., Kronz, A., Simon, K., Spötl, C., Wörner, G., Deininger, M. & Mangini, A., 2011. The significance of chemical, isotopic, and detrital components in three coeval stalagmites from the superhumid southernmost Andes (53°S) as high resolution palaeo-climate proxies. *Quaternary Science Reviews*, 30: 443–459.

Shtober-Zisu, N., Schwarcz, H. P., Chow, T., Omelon, C. R. & Southam, G., 2014. Caves in caves: evolution of post-depositional macroholes in stalagmites. *International Journal of Speleology*, 43: 323–334.

Tremaine, D. M., Froelich, P. N. & Wang, Y., 2011. Speleothem calcite farmed in situ: Modern calibration of $\delta^{18}O$ and $\delta^{13}C$ paleoclimate proxies in a continuously-monitored natural cave system. *Geochimica Cosmochimica Acta*, 75: 4929–4950.

Turkish State Meteorological Service, 2020. *Unpublished Climatic Data from 1980 to 2019, Erdemli/ Mersin 17958 Station*.

Ünal-İmer, E., 2015. *U-series Geochronology and Geochemistry of Vein and Cave Carbonate Deposits in Turkey: the Relationship between Late Quaternary Tectonic and Climatic Events*. Unpublished PhD Thesis, The University of Queensland, 239 pp.

Ünal-İmer, E., Shulmeister, J., Zhao, J., Uysal, I. T. & Feng, Y., 2016. High-resolution trace element and stable/radiogenic isotope profiles of late Pleistocene to Holocene speleothems from Dim Cave, SW Turkey. *Palaeogeography, Palaeoclimatology, Palaeoecology*, 452: 68–79.

Ünal-İmer, E., Shulmeister, J., Zhao, J., Uysal, I. T., Feng, Y., Nguyen, A. D. & Yüce, G., 2015. An 80 kyr-long continuous speleothem record from Dim Cave, SW Turkey with paleoclimatic implications for the Eastern Mediterranean. *Scientific Reports*, 5: 13560

Voarintsoa, N. R. G., Wang, L., Railsback, L. B., Brook, G. A., Liang, F., Cheng, H. & Edwards, R. L., 2017. Multiple proxy analyses of a U/Th-dated stalagmite to reconstruct paleoenvironmental changes in northwestern Madagascar between 370 CE and 1300 CE. *Palaeogeography, Palaeoclimatology, Palaeoecology*, 469: 138–155.

White, W. B., 1988. *Geomorphology and Hydrology of Karst Terrains*. Oxford University Press, Oxford, 480 pp.

White, W. B., 2007. Cave sediments and paleoclimate. *Journal of Cave and Karst Studies*, 69: 76–93.

Zupančič, N., Miler, M., Šebela, S. & Jarc, S., 2016. Application of scanning electron microscopy/energy-dispersive X-ray spectroscopy for characterization of detrital minerals in karst cave speleothems. *Microscopy and Microanalysis*, 22: 87–98.